Physics Letters B 731 (2014) 103–109

Contents lists available at ScienceDirect

Physics Letters B

www.elsevier.com/locate/physletb

Is ρ-meson melting compatible with chiral restoration?

Paul M. Hohler *, Ralf Rapp

Cyclotron Institute and Department of Physics and Astronomy, Texas A&M University, College Station, TX 77843-3366, USA

ARTICLE INFO

Article history:
Received 20 November 2013
Received in revised form 29 January 2014
Accepted 10 February 2014
Available online 15 February 2014
Editor: J.-P. Blaizot

ABSTRACT

Utilizing in-medium vector spectral functions which describe dilepton data in ultra-relativistic heavy-ion collisions, we conduct a comprehensive evaluation of QCD and Weinberg sum rules at finite temperature. The starting point is our recent study in vacuum, where the sum rules have been quantitatively satisfied using phenomenological vector and axial-vector spectral functions which describe hadronic τ-decay data. In the medium, the temperature dependence of condensates and chiral order parameters is taken from thermal lattice QCD where available, and otherwise is estimated from a hadron resonance gas. Since little is known about the in-medium axial-vector spectral function, we model it with a Breit–Wigner ansatz allowing for smooth temperature variations of its width and mass parameters. Our study thus amounts to testing the compatibility of the ρ-broadening found in dilepton experiments with (the approach toward) chiral restoration, and thereby searching for viable in-medium axial-vector spectral functions.

© 2014 The Authors. Published by Elsevier B.V. This is an open access article under the CC BY license (http://creativecommons.org/licenses/by/3.0/). Funded by SCOAP[3].

1. Introduction

The structure of the QCD ground state is reflected in its observable hadron spectrum. In vacuum, the formation of quark and gluon condensates leads to the generation of hadron masses and the spontaneous breaking of chiral symmetry (SBCS). The latter induces mass splittings of ca. 0.5 GeV for chiral partners in the light-hadron spectrum, e.g., between π–σ and ρ–a_1. In a hot medium, chiral symmetry is restored across a region around a pseudo-critical temperature of $T_{\rm pc} \simeq 160$ MeV [1,2]. A long-standing question is how this restoration manifests itself in the hadron spectrum, i.e., what its observable consequences are. Dilepton data from ultra-relativistic heavy-ion collisions (URHICs) [3–5] are now providing strong evidence that the ρ resonance "melts" when the system passes through the pseudo-critical region [6], while experimental access to the in-medium a_1 spectral functions (e.g., via $a_1 \to \pi\gamma$) remains elusive. Thus, to test whether the ρ melting in the vector channel signals chiral restoration, a theoretical evaluation of the in-medium axial-vector spectral function is needed.

A straightforward approach to calculate the in-medium axial-vector spectral function, by using a chiral Lagrangian paralleling the treatment of the ρ meson, turns out to be challenging [7]. For example, the widely used scheme of implementing the ρ and a_1 mesons into the pion Lagrangian through a local gauging procedure causes considerable problems in describing the vacuum spectral functions as measured in hadronic τ decays [8,9], which led some groups to abandon the local gauging procedure [10,11]. In the present work, we adopt a more modest approach to this problem, by utilizing in-medium sum rules. Specifically, we adopt the well-known Weinberg sum rules (WSRs) [13,12,14] which relate (moments of) the difference between vector and axial-vector spectral functions to operators signifying SBCS. Using available calculations of the in-medium ρ spectral function together with temperature dependent order parameters as an input, we ask whether *a* (not necessarily *the*) axial-vector spectral function can be found to satisfy the in-medium sum rules. To tighten our constraints, we simultaneously employ finite-temperature QCD sum rules (QCD-SRs) [15,16] in vector and axial-vector channels, which additionally involve chirally invariant condensates. Related works have been carried out, e.g., in the low-temperature limit [17,18], for heavy-quark channels [19], or focusing on chirally odd condensates in the vector channel only [20].

The present analysis builds on our previous work [21] where QCD and Weinberg sum rules have been tested in vacuum with vector and axial-vector spectral functions that accurately fit hadronic τ-decays. The combination of four WSRs turned out be a rather sensitive probe of the spectral functions, allowing, e.g., to deduce the presence of an excited axial-vector meson, a_1'. This makes for a promising tool at finite temperature (T), aided by an experimentally tested in-medium vector spectral function and in-medium condensates from lattice QCD (lQCD). In the absence of reliable microscopic models for the a_1 and the excited states, the price to pay is the *a priori* unknown in-medium behavior of these states. However, with guidance from model-independent chiral mixing theorems to constrain the T dependence of the higher

* Corresponding author.
E-mail addresses: pmhohler@comp.tamu.edu (P.M. Hohler), rapp@comp.tamu.edu (R. Rapp).

http://dx.doi.org/10.1016/j.physletb.2014.02.021
0370-2693/© 2014 The Authors. Published by Elsevier B.V. This is an open access article under the CC BY license (http://creativecommons.org/licenses/by/3.0/). Funded by SCOAP[3].

states, one can still hope for a sensitive test of the in-medium a_1 spectral function, and to gain novel insights into (the approach to) chiral restoration in the $IJ^P = 11^{\pm}$ chiral multiplet. This is the main objective of our work.

The Letter is organized as follows. We recall the in-medium QCDSRs and WSRs in Section 2 and specify the T dependence of their "right-hand sides" (condensates) in Section 3. The finite-T axial-vector spectral functions ("left-hand sides") are detailed in Section 4, followed by quantitative sum rule analyses in Section 5. We conclude in Section 6.

2. Finite temperature sum rules

The basic quantity figuring into WSRs and QCDSRs is the isovector current–current correlator in the vector (V) and axial-vector (A) channels,

$$\Pi^{\mu\nu}_{V,A}(q^2) = -i\int d^4x e^{ixq}\langle T\vec{J}^{\mu}_{V,A}(x)\vec{J}^{\nu}_{V,A}(0)\rangle. \tag{1}$$

In the quark basis with two light flavors, the currents read $\vec{J}^{\mu}_V = \bar{q}\vec{\tau}\gamma^{\mu}q$ and $\vec{J}^{\mu}_A = \bar{q}\vec{\tau}\gamma^{\mu}\gamma_5 q$, ($\vec{\tau}$: isospin Pauli matrices). From here on, we focus on charge-neutral states (isospin $I_3 = 0$) and drop isospin indices. In vacuum, the currents can be decomposed into 4D transverse and longitudinal components as

$$\Pi^{\mu\nu}_{V,A}(q^2) = \Pi^{T}_{V,A}(q^2)\left(-g^{\mu\nu} + \frac{q^{\mu}q^{\nu}}{q^2}\right) + \Pi^{L}_{V,A}(q^2)\frac{q^{\mu}q^{\nu}}{q^2}. \tag{2}$$

Vector-current conservation implies $\Pi^L_V(q^2) = 0$, while the pion pole induces the partial conservation of the axial-vector current (PCAC),

$$\Pi^L_A(q^2) = f_\pi^2 q^2\delta(q^2 - m_\pi^2). \tag{3}$$

Lorentz symmetry breaking at finite T splits the 4D-transverse polarization functions into 3D-transverse and 3D-longitudinal parts. From here on, we focus on vanishing 3-momentum ($\vec{q} = 0$), for which the 3D components are degenerate. We define pertinent spectral functions as

$$\rho_{V,A} = -\frac{\mathrm{Im}\,\Pi^T_{V,A}}{\pi}, \qquad \rho_{\bar{A}} = \rho_A - \frac{\mathrm{Im}\,\Pi^L_A}{\pi}. \tag{4}$$

The QCDSRs equate a dispersion integral on the left-hand-side (LHS) to an operator product expansion (OPE) on the right-hand-side (RHS); for the axial-vector channels they read [22–24]

$$\begin{aligned}
&\frac{1}{M^2}\int_0^{\infty} ds\,\frac{\rho_{V,\bar{A}}(s)}{s}e^{-s/M^2} \\
&= \frac{1}{8\pi^2}\left(1 + \frac{\alpha_s}{\pi}\right) + \frac{m_q\langle\bar{q}q\rangle}{M^4} + \frac{1}{24M^4}\left\langle\frac{\alpha_s}{\pi}G^2_{\mu\nu}\right\rangle \\
&\quad - \frac{\pi\alpha_s}{M^6}\frac{(56,-88)}{81}\langle\mathcal{O}^{V,A}_4\rangle + \sum_h\frac{\langle\mathcal{O}^{d=4,\tau=2}_h\rangle_T}{M^4} \\
&\quad + \frac{\langle\mathcal{O}^{d=6,\tau=2}_h\rangle_T}{M^6} + \frac{\langle\mathcal{O}^{d=6,\tau=4}_h\rangle_T}{M^6}\ldots,
\end{aligned} \tag{5}$$

where the space-like q^2 is traded for the Borel mass M^2 by a standard Borel transform. On the RHS, we include all operators up to dimension-6, i.e., the common scalar operators already present in the vacuum (quark, gluon, and 4-quark condensates, $\langle\bar{q}q\rangle$, $\langle\frac{\alpha_s}{\pi}G^2_{\mu\nu}\rangle$, and $\langle\mathcal{O}^{V,A}_4\rangle$, respectively), as well as non-scalar operators induced by thermal hadrons (h), organized by dimension (d) and twist (τ). The T dependencies are detailed in Section 3.

The WSRs relate moments of the difference between the vector and axial-vector spectral functions to chiral order parameters. Their formulation at finite T was first carried out in Ref. [14]. Subtracting the two channels of the finite-T QCDSRs from one another, Taylor-expanding the Borel exponential, and equating powers of M^2 on each side of the sum rule yields

$$\text{(WSR1)} \quad \int_0^{\infty} ds\,\frac{\Delta\rho(s)}{s} = f_\pi^2, \tag{6}$$

$$\text{(WSR2)} \quad \int_0^{\infty} ds\,\Delta\rho(s) = f_\pi^2 m_\pi^2 = -2m_q\langle\bar{q}q\rangle, \tag{7}$$

$$\text{(WSR3)} \quad \int_0^{\infty} ds\,s\Delta\rho(s) = -2\pi\alpha_s\langle\mathcal{O}^{\mathrm{SB}}_4\rangle, \tag{8}$$

where $\Delta\rho = \rho_V - \rho_A$. The chiral breaking 4-quark condensate is given by the axial-vector ones as

$$\langle\mathcal{O}^{\mathrm{SB}}_4\rangle = \frac{16}{9}\left(\frac{7}{18}\langle\mathcal{O}^V_4\rangle + \frac{11}{18}\langle\mathcal{O}^A_4\rangle\right). \tag{9}$$

Since the WSRs only contain chiral order parameters, they are particularly sensitive to chiral symmetry restoration, whereas the QCDSRs are channel specific thus providing independent information.

3. In-medium condensates

We now turn to the T dependence of each condensate figuring into the QCDSRs. To leading order in the density of a hadron h in the heat bath, the in-medium condensate associated with a given operator $\mathcal{O}$ can be approximated by

$$\langle\mathcal{O}\rangle_T \simeq \langle\mathcal{O}\rangle_0 + d_h\int\frac{d^3k}{(2\pi)^3 2E_h}\langle h(\vec{k})|\mathcal{O}|h(\vec{k})\rangle n_h(E_h), \tag{10}$$

where $\langle\mathcal{O}\rangle_0$ is the vacuum value of the operator, $\langle h(\vec{k})|\mathcal{O}|h(\vec{k})\rangle$ its hadronic matrix element, $E_h^2 = m_h^2 + \vec{k}^2$, and d_h, m_h, and n_h are the hadron's spin–isospin degeneracy, mass, and thermal distribution function (Bose (n_b) or Fermi (n_f)), respectively. Working at zero baryon chemical potential ($\mu_B = 0$), we absorb anti-baryons into the degeneracy factor of baryons. Corrections to Eq. (10) figure via multi-hadron matrix elements of the operator.

We approximate the medium by a hadron resonance gas (HRG) including all confirmed states with mass $m_h \leqslant 2$ GeV [25]. For the temperatures of interest here, $T \lesssim 170$ MeV, the HRG is known to reproduce the equation of state from lQCD quite well [26]. Since the calculation of the in-medium ρ spectral function is also based on HRG degrees of freedom, the OPE and spectral function sides of the sum rules are evaluated in the same basis. For the subsequent discussion, we define the integrals

$$I^h_n = d_h\int\frac{d^3k}{(2\pi)^3 E_h}k^{2n-2}n_h(E_h). \tag{11}$$

Note that $m_h I^h_1$ is the scalar density, ϱ^h_s.

3.1. Quark condensate

The HRG correction to the quark condensate is [27,28]

$$\frac{\langle\bar{q}q\rangle_T}{\langle\bar{q}q\rangle_0} = 1 - \frac{\varrho^{\pi}_s}{2m_\pi f_\pi^2} - \frac{\varrho^{K}_s}{4m_K f_K^2} - \frac{\varrho^{\eta}_s}{6m_\eta f_\eta^2} - \frac{\varrho^{\eta'}_s}{3m_{\eta'} f_{\eta'}^2}$$

Table 1
Numerical values of key parameters figuring into Eq. (12). For hadron masses not listed we take averages from the particle data group [25].

Parameter	f_π	f_K	f_η	$f_{\eta'}$	m_q	m_π
Value (MeV)	92.4	113	124	107	7	139.6

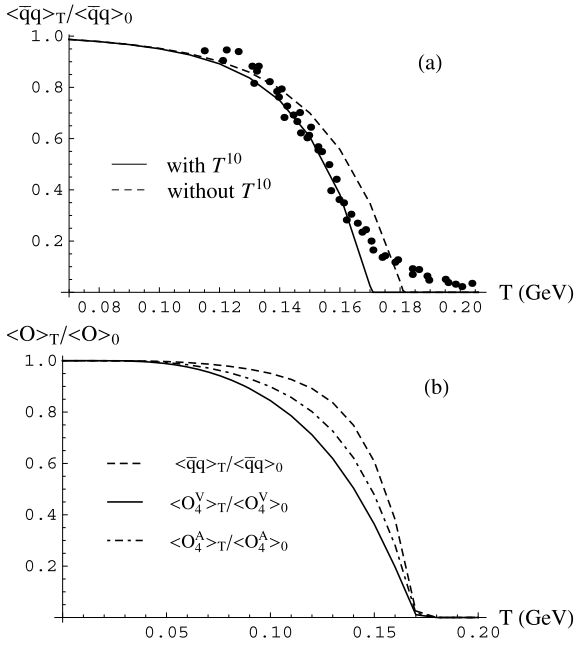

Fig. 1. Temperature dependence of: (a) the quark condensate relative to its vacuum value, compared to thermal lQCD data [1]; (b) axial-vector 4-quark condensates relative to their vacuum values, compared to the quark condensate.

$$-\sum_B \frac{\sigma_B}{f_\pi^2 m_\pi^2}\varrho_s^B - \sum_M \frac{\sigma_M}{f_\pi^2 m_\pi^2}\varrho_s^M - \alpha T^{10}. \tag{12}$$

The Goldstone boson contribution can be inferred from current algebra (with decay constants given in Table 1). The contributions from baryons (B) and other mesons (M) can be derived from the HRG partition function via $\partial \ln Z/\partial m_q$, which is nothing but the in-medium condensate. They are determined by their σ-terms which to lowest order are given by the (current) quark masses, m_q, of the light valence quarks in the hadron [29]. However, important contributions arise from the hadron's pion cloud [30,31]. We write

$$\sigma_h = \sigma_q^{\text{bare}} + \sigma_\pi^{\text{cloud}} \equiv \sigma_0 m_q (N_q - N_s) \tag{13}$$

where N_q (N_s) is the number of all (strange) valence quarks in h. We adjust the proportionality constant to $\sigma_0 = 2.81$, to recover the recent value, $\sigma_N = 59$ MeV [32], of the nucleon and assume it to be universal for all hadrons. This leads to fair agreement with estimates of σ_h for other ground-state baryons [32]. Note that the decomposition of the σ terms into quark core and pion cloud effects parallels the medium effects of the ρ spectral function [33].

Our HRG results reproduce lQCD "data" [1] for $T \lesssim 140$ MeV, see Fig. 1(a). To improve the agreement at higher T without affecting the low-T behavior, we introduced a term αT^{10} on the RHS of Eq. (12), with $\alpha = 1.597 \cdot 10^7$ GeV^{-10}. The quark condensate then vanishes slightly above $T = 170$ MeV, signaling the breakdown of our approach. Choosing a somewhat higher power in T (with accordingly adjusted α) has no significant impact on our results, while a smaller power adversely affects the agreement with lQCD data at low T.

3.2. Gluon condensate

For the gluon condensate, the contributions from pions and nucleons have been evaluated in Refs. [34,22,24]. The HRG effect can be inferred from the trace anomaly,

$$\theta_\mu^\mu = -\frac{9}{8}\frac{\alpha_s}{\pi}G_{\mu\nu}^2 + \sum_q m_q \bar{q}q, \tag{14}$$

by calculating $\Delta\langle\theta_\mu^\mu\rangle = \epsilon - 3P = \sum_h m_h \varrho_s^h$ to obtain

$$\Delta\left\langle\frac{\alpha_s}{\pi}G_{\mu\nu}^2\right\rangle = -\frac{8}{9}\left[\Delta\langle\theta_\mu^\mu\rangle - 2m_q\Delta\langle\bar{q}q\rangle - m_s\Delta\langle\bar{s}s\rangle\right]. \tag{15}$$

The change in light-quark condensate is taken from Eq. (12). For the strange-quark condensate, we assume its suppression from individual resonances to scale with the valence strange-quark content of each hadron h, paralleling the procedure of determining the σ-term for each hadron. One has

$$m_s\Delta\langle\bar{s}s\rangle = \sum_h \frac{N_s}{N_q - N_s}\left(2m_q\Delta\langle\bar{q}q\rangle_h\right), \tag{16}$$

where $\Delta\langle\bar{q}q\rangle_h$ is from Eq. (12). The HRG suppression of the gluon condensate reaches 13% at $T = 170$ MeV.

3.3. Four-quark condensates

For medium dependence of the vector and axial-vector 4-quark condensates induced by Goldstone bosons, we adopt the results from current algebra [22]. For the non-Goldstone bosons and baryons, arguments based on the large-N_c limit [35,28] suggest a factorization approximation, i.e., the medium effect linear in their (scalar) density amounts to a factor of 2 times the reduction in the quark condensate, with the same factorization parameter as in vacuum (we have checked that an increase of the in-medium factorization parameter by a factor of 2 has a negligible impact on the OPEs and thus on the resulting spectral functions). The T dependence of the vector and axial-vector 4-quark condensates then takes the form

$$\frac{\langle\mathcal{O}_4^{V,A}\rangle_T}{\langle\mathcal{O}_4^{V,A}\rangle_0} = 1 - \frac{(12/7, 12/11)}{m_\pi f_\pi^2}\varrho_s^\pi - \frac{(9/14, 9/22)}{m_K f_K^2}\varrho_s^K - \sum_B \frac{2\sigma_B}{f_\pi^2 m_\pi^2}\varrho_s^B - \sum_M \frac{2\sigma_M}{f_\pi^2 m_\pi^2}\varrho_s^M + \beta_{V,A}T^{10}. \tag{17}$$

As for the quark condensate, we augmented the T dependence by a term $\beta_{V,A}T^{10}$. Since thermal lQCD data are not available for 4-quark condensates, we adjusted $\beta_{V,A}$ for each channel to render them vanishing at the same temperature as the quark condensate, resulting in $\beta_V = 3.05 \cdot 10^7$ GeV^{-10} and $\beta_A = 1.74 \cdot 10^7$ GeV^{-10}. The T dependence of the chiral breaking 4-quark condensate follows from the axial-vector ones via Eq. (9); relative to the quark condensate, their initial fall-off is faster but slows down above $T \simeq 140$ MeV, cf. Fig. 1(b).

3.4. Non-scalar condensates

Hadrons in the heat bath also induce non-scalar condensates. For our QCDSR analysis the relevant ones are of dimension-4 twist-2 $\langle\mathcal{O}^{d=4,\tau=2}\rangle_T$, dimension-6 twist-2 $\langle\mathcal{O}^{d=6,\tau=2}\rangle_T$, and dimension-6 twist-4 $\langle\mathcal{O}^{d=6,\tau=4}\rangle_T$. We adopt their T dependence as elaborated in Refs. [22–24], given by each hadron as

$$\langle \mathcal{O}_h^{d=4,\tau=2}\rangle_T = \frac{A_2^h}{4}\left(m_h^2 I_1^h + \frac{4}{3} I_2^h\right),$$
$$\langle \mathcal{O}_h^{d=6,\tau=2}\rangle_T = -\frac{5A_4^h}{24}\left(m_h^4 I_1^h + 4m_h^2 I_2^h + \frac{16}{5} I_3^h\right),$$
$$\langle \mathcal{O}_h^{d=6,\tau=4}\rangle_T = \frac{B_2^h}{4}\left(m_h^2 I_1^h + \frac{4}{3} I_2^h\right). \tag{18}$$

The parameters A_2 and A_4, which control the twist-2 operators, are related to moments of parton distribution functions for the u and d quarks in the hadron

$$A_n = 2\int_0^1 dx\, x^{n-1}\left(\bar{q}(x) + q(x)\right). \tag{19}$$

One can think of A_2 as twice the momentum fraction of the up and down quarks in the hadron, with A_4 a higher moment. Their values are reasonably well known for the pion and nucleon, $A_2^\pi = 0.97$, $A_4^\pi = 0.255$, $A_2^N = 1.12$, $A_4^N = 0.12$, while there is substantial uncertainty for other hadrons. For baryons, we assume A_2 and A_4 to be identical to the nucleon values, but weighted by the light-quark fraction; e.g., the A_2 of the Λ is $\frac{2}{3}A_2^N$. The kaons and etas are approximated with the pion's parton distribution functions, reduced by the strange-quark content. For other mesons, Eq. (19) is used with the nucleon parton distributions functions, rescaled by the valence-quark content and also reduced by the strange-quark content. This gives $A_2 = 0.801$ and $A_4 = 0.086$ for non-strange mesons. The B_2's are related to integrals of the twist-4 part of the spin-averaged (longitudinal) structure function, $F_{2(L)}^{\tau=4}$ [36,23]. For the nucleon, it has been extracted as $B_2^N = -0.247$ GeV^2. Since there is no empirical information for other hadrons, we assume their B_2 to be the same as for the nucleon (suppressed by the strange-quark content); varying it by a factor of 2 produces no noticeable changes in the final spectral functions. Gluonic contributions are believed to be numerically insignificant [22,23] and have been neglected.

4. Finite temperature spectral functions

Our starting point are the vacuum axial-vector spectral functions of Ref. [21].[1] They are comprised of contributions from the ground state (ρ and a_1 peaks), a first excited state (ρ' and a_1'), and a chirally invariant (i.e., identical) continuum for both channels. The vacuum ρ is taken from the microscopic model of Ref. [37], while a_1, ρ' and a_1' are parameterized with Breit–Wigner functions. For the present analysis, we have slightly modified the vacuum parameters of the ρ' to shift its threshold energy to higher energies. This avoids its low-mass tail to reach well below 1 GeV where the τ-decay data do not exhibit any 4π contributions. The modification to the ρ' formfactor is compensated by a small modification of the mass and width of the a_1' as to recover a near-perfect agreement with WSR-1 and WSR-2. The re-evaluation of the vacuum QCDSRs requires numerical values of 4-quark factorization parameter of $\kappa = 2.1$ in $\langle \mathcal{O}_4^{\rm SB}\rangle = \frac{16}{9}\kappa\langle\bar{q}q\rangle^2$, and of the gluon condensate of $\langle \frac{\alpha_s}{\pi} G_{\mu\nu}^2\rangle = 0.017$ GeV^4. The updated vacuum spectral functions, shown in Fig. 2, are very similar to the ones in Ref. [21].

[1] The normalization used in Eq. (25) of Ref. [21] for the Breit–Wigner width of the a_1 peak contained a (small) imaginary contribution; we have corrected this and could recover the same level of agreement with the experimental data and sum rules with a minor modification of the parameters.

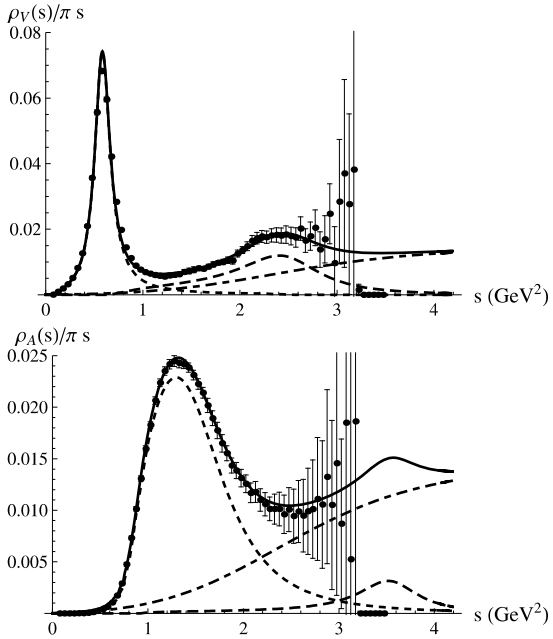

Fig. 2. Vacuum spectral functions in the vector (top) and axial-vector (bottom) channels, compared to experimental data for hadronic τ decays [8]; The total spectral function in each channel (solid curve) is composed of a ground state (dotted curve), excited resonance (dashed curve), and a universal continuum (dot-dashed curve).

Finite-temperature effects in the spectral functions are implemented as follows. For the ρ meson, we employ the microscopic calculations using hadronic effective theory [38] at vanishing baryon chemical potential. This is the key input to our analysis, as these spectral functions are consistent with dilepton data in URHICs [6], and thus provide a direct link to experiment. The only amendment we allow is a reduction of the vector-dominance coupling strength (as routinely done in QCDSR analyses [22,24,39,40]). Optimal agreement with the QCDSR requires a reduction of up to 7% at $T = 170$ MeV.

For the a_1 meson, the lack of quantitative calculations at finite T leads us to parameterize the medium modifications of its spectral function. We introduce four parameters which control the a_1 peak's location, width, and strength in-medium. For the a_1 mass, we write $M_{a_1}^T = M_{a_1}(1 - \delta M_{a_1}(T)/M_{a_1})$, and for the current coupling $C_{a_1}^T = C_{a_1}(1 - \delta C_{a_1}(T)/C_{a_1})$. The width is increased and extended below the vacuum threshold by adding the following term to the vacuum width, $\Gamma_{a_1}(s)$,

$$\Delta\Gamma_{a_1}(s) = \left(\Gamma_1^T + \frac{s}{M_{a_1}^2}\Gamma_2^T\right)\left(\frac{\Lambda_{a_1}^2 + M_{a_1}^2}{\Lambda_{a_1}^2 + s}\right)^2 \tag{20}$$

where Γ_1^T and Γ_2^T are T-dependent constants, and the last factor is a formfactor with the same scale, Λ_{a_1}, as in vacuum. The resulting ground-state axial-vector spectral function in medium takes the form

$$\rho_{a_1}(s,T) = \frac{1}{\pi} C_{a_1}^T \frac{\sqrt{s}\Gamma_{a_1}^T(s,T)}{(s - M_{a_1}^{T2})^2 + s\Gamma_{a_1}^T(s,T)^2}, \tag{21}$$

with $\Gamma_{a_1}^T(s,T) = \Gamma_{a_1}(s) + \Delta\Gamma_{a_1}(s)$.

The temperature dependence of the excited states is even less known. Instead of introducing additional parameters for their in-medium Breit–Wigners (which are hard to control), we rather apply the model independent low-temperature effect known as chiral mixing [41,42] to the ρ' and a_1' states. However, in the spirit of the HRG, we go beyond the mixing induced by only thermal pions

by including the effect from the virtual pion cloud of the thermal hadrons. This effect has been worked out for the pion cloud of the nucleon in cold nuclear matter [43,44]. To extend it to other hadrons (not including the non-pion Goldstone bosons), we define a mixing parameter

$$\hat{\epsilon}_h(T) = \frac{4}{3}\frac{\sigma_\pi^{\rm cloud}}{f_\pi^2 m_\pi^2}\varrho_s^h. \tag{22}$$

The total mixing parameter, $\hat{\epsilon}$, is the sum of the individual $\hat{\epsilon}_h$ plus that of the pion, $\hat{\epsilon}_\pi = 2\varrho_s^\pi/(3m_\pi f_\pi^2)$. As with the quark condensates, we introduce an additional T^{10}-term to render $\hat{\epsilon} = 1/2$ at the temperature where $\langle\bar{q}q\rangle_T = 0$. The in-medium spectral functions for the excited axial-vector states then follow as

$$\begin{aligned}\rho_{V'}(T) &= \big[1-\hat{\epsilon}(T)\big]\rho_{V'}^{\rm vac} + \hat{\epsilon}(T)\rho_{A'}^{\rm vac} + \frac{1}{2}\hat{\epsilon}(T)\rho_{a_1}^{\rm vac},\\ \rho_{A'}(T) &= \big[1-\hat{\epsilon}(T)\big]\rho_{A'}^{\rm vac} + \hat{\epsilon}(T)\rho_{V'}^{\rm vac}.\end{aligned} \tag{23}$$

The a_1 contribution to the excited vector channel admixes only the part which is not included in the microscopic calculation of the ρ, see Ref. [45] for details. Our approximate extension of the mixing beyond the low-T pion gas limit is only carried linear in the (scalar) hadron densities, but in line with the in-medium treatment of the condensates. However, no finite-momentum nor finite-mass effects of the (virtual) pions have been accounted for.

The chirally invariant continuum is assumed to be T-independent (e.g., chiral mixing would not affect it).

Lastly, we need to address the T dependence of the 4D longitudinal part of the axial-vector spectral function, i.e., the pion pole. We approximate the pion mass by the leading-order prediction of chiral perturbation theory,

$$m_\pi^2(T) = m_\pi^2\left(1+\frac{1}{4}\hat{\epsilon}_\pi(T)\right), \tag{24}$$

i.e., induced by the pion gas only. This produces a weak T dependence as expected for a Goldstone boson. Assuming the Gell-Mann–Oakes–Renner relation to hold at finite T, allows us to infer $f_\pi(T)$ from the above-constructed T-dependence of the quark condensate.

To summarize this section, we have supplemented a microscopic model for the ρ spectral function with a 4-parameter ansatz for the in-medium a_1, chiral mixing for the excited states, and a weakly T-dependent pion mass from chiral perturbation theory. We now investigate whether this setup can satisfy QCDSRs and WSRs.

5. Finite-temperature sum rule analysis

Let us start by describing the quantitative criteria which govern the numerical values of the in-medium a_1 parameters introduced in the previous section.

To evaluate the QCDSRs, we adopt the conventional method of Refs. [46,39] to calculate an average deviation between the LHS and RHS over a suitable Borel window, referred to as a d-value. The same procedure and Borel window criteria as for the vacuum analysis in Ref. [21] are adopted. A d-value of below 1% has been argued to reasonably bracket remaining uncertainties in the matching procedure [39]; we adopt this as our figure of merit in both A and V channels below.

To evaluate the WSRs, we define a similar measure of deviation between the two sides as

$$d_{\rm WSR} = \frac{\rm LHS - RHS}{\rm RHS}. \tag{25}$$

Table 2
Summary of deviation measures for QCDSRs (upper 2 lines) and WSRs (lower 6 lines) at finite temperature.

T [MeV]	0	100	140	150	160	170
d_V (%)	0.59	0.43	0.44	0.49	0.57	0.67
d_A (%)	0.49	0.48	0.56	0.59	0.55	0.56
$d_{\rm WSR1}$ (%)	∼0	0.003	0.04	0.04	−0.004	0.004
$d_{\rm WSR2}$ (%)	∼0	−0.0002	−0.0008	−0.002	−0.0003	−0.005
$d_{\rm WSR3}$ (%)	200	181	258	372	585	11 600
r_{-1}	1	0.96	0.72	0.57	0.37	0.14
r_0	1	0.93	0.66	0.50	0.31	0.12
r_1	1	0.91	0.64	0.50	0.32	0.15

This measure is much simpler than the QCDSR analog because it does not involve any Borel window. However, it also has its subtleties. The integrands of the LHS of each WSR are oscillatory functions with appreciable cancellations to yield the RHS (cf. Fig. 2 in Ref. [21]), especially for the higher moments. Since we only use a finite number of moments (3), this could, in principle, lead to "fine-tuned solutions" to the WSRs where the oscillations are still large, and thus $\rho_V(s) \neq \rho_A(s)$ even close to restoration. To probe this behavior (and thus the sensitivity to any "artificial" fine tuning), we introduce an "absolute-value" version of the LHS by

$$\tilde{w}_n(T) \equiv \int_0^\infty ds\, s^n \big|\Delta\rho(s;T)\big|. \tag{26}$$

Though these moments are not directly related to chiral order parameters, they should diminish toward restoration. We define pertinent ratios $r_n = \tilde{w}_n(T)/\tilde{w}_n(T=0)$.

Our analysis proceeds as follows. We first evaluate the QCDSR for the vector channel. With a small reduction in the vector dominance coupling, we find acceptable d_V values ranging from 0.43% to 0.67% for all $T = 0$–170 MeV (cf. Table 2). This is a nontrivial result by itself. For the axial-vector channel, the QCDSRs and two WSRs are used simultaneously to search for in-medium a_1 parameters which minimize

$$f = d_{\rm WSR1}^2 + d_{\rm WSR2}^2 + d_A^2, \tag{27}$$

while requiring a smooth T dependence. The thus obtained finite-T axial-vector spectral functions are shown in Fig. 3. For all cases, the percentage deviation of WSR-1 and WSR-2 is below 0.1%, and d_A remains below 0.6%. Deviations of WSR-3 are much larger, but comparable to the vacuum up to $T \simeq 150$ MeV. At $T = 160$ and especially 170 MeV, the magnitude of the RHSs is small and enters into the denominator of $d_{\rm WSR}$, thus greatly magnifying residual deviations. The r_n measures decrease monotonically with T suggesting acceptable deviations even for WSR-3. We therefore conclude that our spectral functions are compatible with both QCDSRs and WSRs.

To probe the uncertainties in our method, we depict in Fig. 4 ranges of axial-vector spectral functions with relaxed constraints, at an intermediate temperature of $T = 150$ MeV. The dashed lines border a regime of spectral functions which are obtained by only requiring $d_A = 1\%$ for the axial-vector QCDSR (the band could be larger if all spectral functions with $d_A < 1\%$ were included). From this collection of curves, we then select those whose agreement with WSR1 is within 1%, producing a much narrower (shaded) region bordered by dotted lines. The *combined* constraints of QCDSRs and WSRs are thus shown to noticeably increase the selectivity of the in-medium axial-vector spectral function.

A visual inspection of the in-medium spectral functions supports the trend toward restoration, cf. Fig. 3: the a_1 peak gradually

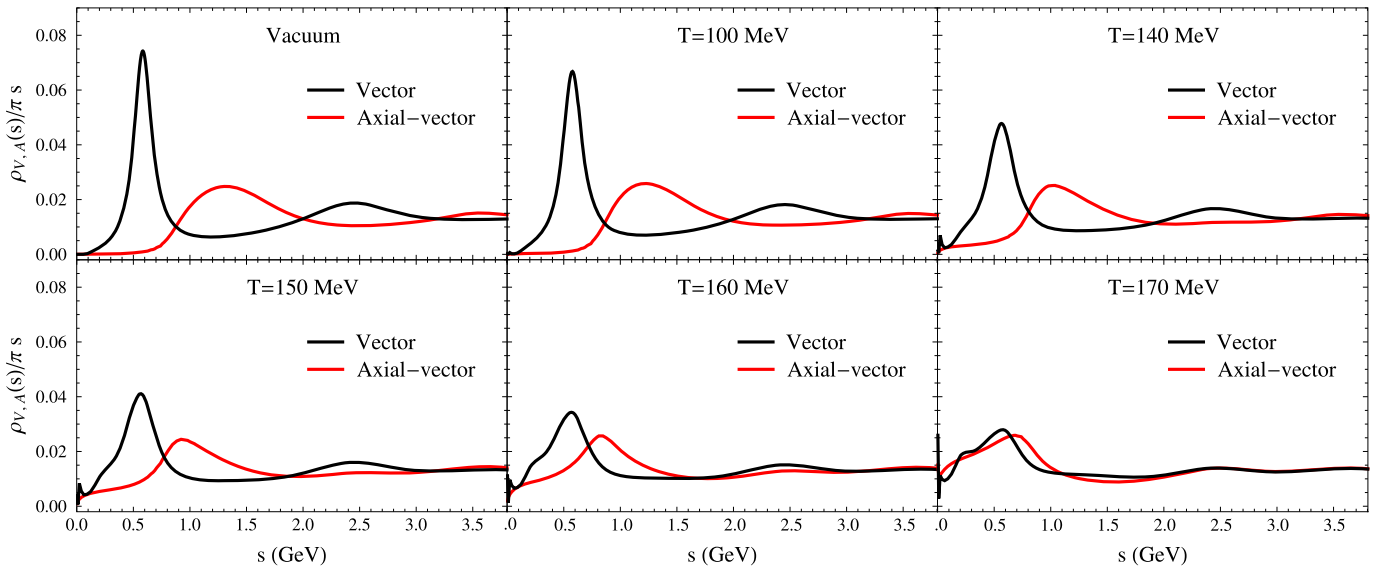

Fig. 3. Finite-temperature vector (black curve) and axial-vector (red curve) spectral functions. (For interpretation of the references to color in this figure legend, the reader is referred to the web version of this article.)

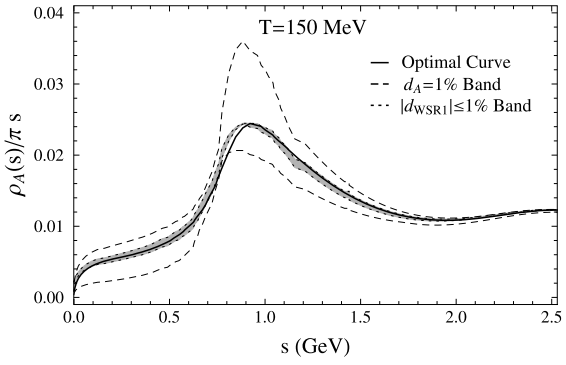

Fig. 4. Regions of axial-vector spectral functions at $T = 150$ MeV when requiring agreement with the QCDSR only at $d_A = 1\%$ (dashed lines), and additionally with WSR-1 at $|d_{\mathrm{WSR1}}| \leqslant 1\%$ (dotted lines). The solid line corresponds to a minimal f value from Eq. (27).

merges into the ρ while the excited states degenerate somewhat earlier through chiral mixing. The ρ–a_1 merging is largely dictated by the WSRs, but the concrete shape close to chiral restoration is more sensitive to the QCDSRs. Note that our analysis not only complies with a "trivial" degeneracy at the restoration point, but rather provides a systematic temperature evolution, starting from the vacuum, compatible with current best estimates for the T dependent chiral order parameters and condensates (at $T = 170$ MeV, our condensates are close to zero, undershooting the lQCD data for the 2-quark condensate; our axial-vector spectral function at this temperature is thus more of an illustration of the expected degeneracy at higher T where $\langle\bar{q}q\rangle_T \simeq 0$). The in-medium a_1 mass shift is consistent with a leading T^4 behavior, in line with model-independent constraints from the chiral Lagrangian. Our analysis also suggests that the approach toward restoration "burns off" the chiral mass splitting between the ρ and a_1, while "bare" masses of $m_0 \simeq 0.8$ GeV essentially persist, similar to Ref. [7].

6. Conclusion

The objective of this work was to test whether in-medium vector spectral functions which describe dilepton data in heavy-ion collisions are compatible with chiral symmetry restoration. Toward this end, we deployed QCD and Weinberg sum rules in a combined analysis of vector and axial-vector spectral functions, using lattice-QCD and the hadron resonance gas to estimate the in-medium condensates and chiral order parameters, and chiral mixing to treat the T dependence of excited states. We first found that the QCDSR in the vector channel is satisfied with a small (order 5%) amendment of vector dominance. We then introduced a 4-parameter ansatz for the in-medium a_1 spectral function and found that a smooth reduction of its mass (approaching the ρ mass) and large increase in width (accompanied by a low-mass shoulder) can satisfy the axial-vector QCDSR and 3 WSRs over the entire temperature range from $T = 0$–170 MeV, ultimately merging with the vector channel. This establishes a direct connection between dileptons and chiral restoration, and thus the answer to the originally raised question is positive. Our findings remain to be scrutinized by microscopic calculations of the a_1 spectral function. Work in this direction is ongoing.

Acknowledgements

This work is supported by the US NSF under grant No. PHY–1306359 and by the Alexander von Humboldt Foundation (Germany).

References

[1] S. Borsanyi, et al., Wuppertal-Budapest Collaboration, J. High Energy Phys. 1009 (2010) 073.
[2] A. Bazavov, et al., Phys. Rev. D 85 (2012) 054503.
[3] R. Arnaldi, et al., NA60 Collaboration, Eur. Phys. J. C 61 (2009) 711.
[4] D. Adamova, et al., CERES/NA45 Collaboration, Phys. Lett. B 666 (2008) 425.
[5] F. Geurts, et al., STAR Collaboration, Nucl. Phys. A 904–905 (2013) 217c.
[6] R. Rapp, PoS CPOD2013 (2013) 008.
[7] M. Urban, M. Buballa, J. Wambach, Phys. Rev. Lett. 88 (2002) 042002.
[8] R. Barate, et al., ALEPH Collaboration, Eur. Phys. J. C 4 (1998) 409.
[9] K. Ackerstaff, et al., OPAL Collaboration, Eur. Phys. J. C 7 (1999) 571.
[10] M. Urban, M. Buballa, J. Wambach, Nucl. Phys. A 697 (2002) 338.
[11] D. Parganlija, F. Giacosa, D.H. Rischke, Phys. Rev. D 82 (2010) 054024.
[12] S. Weinberg, Phys. Rev. Lett. 18 (1967) 507.
[13] T. Das, V.S. Mathur, S. Okubo, Phys. Rev. Lett. 19 (1967) 859.
[14] J.I. Kapusta, E.V. Shuryak, Phys. Rev. D 49 (1994) 4694.
[15] M.A. Shifman, A.I. Vainshtein, V.I. Zakharov, Nucl. Phys. B 147 (1979) 385.
[16] M.A. Shifman, A.I. Vainshtein, V.I. Zakharov, Nucl. Phys. B 147 (1979) 448.
[17] E. Marco, R. Hofmann, W. Weise, Phys. Lett. B 530 (2002) 88.
[18] N.P.M. Holt, P.M. Hohler, R. Rapp, Phys. Rev. D 87 (2013) 076010.

[19] T. Hilger, B. Kampfer, S. Leupold, Phys. Rev. C 84 (2011) 045202.
[20] T. Hilger, R. Thomas, B. Kampfer, S. Leupold, Phys. Lett. B 709 (2012) 200.
[21] P.M. Hohler, R. Rapp, Nucl. Phys. A 892 (2012) 58.
[22] T. Hatsuda, Y. Koike, S.-H. Lee, Nucl. Phys. B 394 (1993) 221.
[23] S. Leupold, U. Mosel, Phys. Rev. C 58 (1998) 2939.
[24] S. Zschocke, O.P. Pavlenko, B. Kämpfer, Eur. Phys. J. A 15 (2002) 529.
[25] K. Nakamura, et al., Particle Data Group, J. Phys. G 37 (2010) 075021.
[26] F. Karsch, K. Redlich, A. Tawfik, Eur. Phys. J. C 29 (2003) 549.
[27] P. Gerber, H. Leutwyler, Nucl. Phys. B 321 (1989) 387.
[28] S. Leupold, J. Phys. G 32 (2006) 2199.
[29] J. Gasser, H. Leutwyler, M.E. Sainio, Phys. Lett. B 253 (1991) 252.
[30] I. Jameson, A.W. Thomas, G. Chanfray, J. Phys. G 18 (1992) L159.
[31] M.C. Birse, J.A. McGovern, Phys. Lett. B 292 (1992) 242.
[32] J. Martin Camalich, L.S. Geng, M.J. Vicente Vacas, Phys. Rev. D 82 (2010) 074504.
[33] R. Rapp, J. Phys. Conf. Ser. 420 (2013) 012017.
[34] T.D. Cohen, R.J. Furnstahl, D.K. Griegel, Phys. Rev. C 45 (1992) 1881.
[35] S. Leupold, Phys. Lett. B 616 (2005) 203.
[36] S. Choi, T. Hatsuda, Y. Koike, S.H. Lee, Phys. Lett. B 312 (1993) 351.
[37] M. Urban, M. Buballa, R. Rapp, J. Wambach, Nucl. Phys. A 641 (1998) 433.
[38] R. Rapp, J. Wambach, Eur. Phys. J. A 6 (1999) 415.
[39] S. Leupold, W. Peters, U. Mosel, Nucl. Phys. A 628 (1998) 311.
[40] S. Leupold, Phys. Rev. C 64 (2001) 015202.
[41] M. Dey, V.L. Eletsky, B.L. Ioffe, Phys. Lett. B 252 (1990) 620.
[42] J.V. Steele, H. Yamagishi, I. Zahed, Phys. Lett. B 384 (1996) 255.
[43] G. Chanfray, J. Delorme, M. Ericson, Nucl. Phys. A 637 (1998) 421.
[44] B. Krippa, Phys. Lett. B 427 (1998) 13.
[45] H. van Hees, R. Rapp, Nucl. Phys. A 806 (2008) 339.
[46] D.B. Leinweber, Ann. Phys. 254 (1997) 328.